Low-Field de Haas-van Alphen Effect in Zinc*†

A. S. JOSEPH‡ AND W. L. GORDON

Case Institute of Technology, Cleveland, Ohio

(Received December 11, 1961)

A study of the low-field de Haas-van Alphen effect in zinc, employing automatic recording of the variation of the torque as a function of the reciprocal of the applied magnetic field, has revealed six sets of periods. These periods are assigned in a consistent manner to portions of the free-electron (single orthogonalized plane-wave) model of the Fermi surface. Cyclotron masses associated with the three larger sets of observed periods are found to agree well with the theoretical estimates. Evidence is obtained for the presence of a spin-orbit energy gap across the hexagonal face of the first Brillouin zone near the corners. Thus, the validity of the single Brillouin-zone construction is demonstrated for zinc.

INTRODUCTION

WHEN a single crystal of metal is suspended in a magnetic field, H, at liquid helium temperatures, it is found that the diamagnetic portion of its susceptibility, χ, becomes a periodic oscillatory function of the reciprocal of the magnetic field strength. This phenomenon is known as the de Haas-van Alphen effect (DHVA).

Although Landau[1] was the first to show that the diamagnetic susceptibility at very low temperature should indeed be a periodic function of $1/H$, it was Onsager,[2] and later on Lifshitz and Kosevich[3] in a more detailed analysis, who derived the presently accepted theory of the DHVA effect. The result of Lifshitz and Kosevich gave $\chi_\perp$ in a direction perpendicular to the magnetic field as

$$\chi_\perp = -\frac{(e\hbar/c)^{\frac{1}{2}}}{\pi(2\pi)^{\frac{1}{2}}\hbar^3}\frac{kT}{H^{\frac{1}{2}}}\frac{\partial S_m}{\partial \theta}\left|\frac{\partial^2 S_m}{\partial P_z^2}\right|^{-\frac{1}{2}}$$

$$\times \sum_l \left[\sin\left(\frac{lcS_m}{e\hbar H}\mp\frac{\pi}{4}-2\pi l\gamma\right)\cos\left(\frac{l}{2m_0}\frac{dS_m}{d\zeta}\right) \right.$$

$$\left. \div l^{\frac{1}{2}}\sinh\left(\frac{l\pi ckT}{e\hbar H}\frac{dS_m}{d\zeta}\right) \right]. \quad (1)$$

The symbols are defined as: $S_m=$ the extremal cross section of the Fermi surface in momentum space cut by planes perpendicular to H, $P_z=$ momentum of electrons in the H direction, $\theta=$ an angular coordinate in a plane perpendicular to the axis of suspension of the specimen, $m_0=$ free electron mass, $\zeta=$ Fermi energy, $(1/2\pi)(dS_m/d\zeta)=m^*$ (cyclotron mass), and $\sum_l=$ sum-

[1] L. Landau, Z. Physik 64, 629 (1930); Appendix to D. Shoenberg, Proc. Roy. Soc. (London) A170, 341 (1939).
[2] L. Onsager, Phil. Mag. 43, 1006 (1952).
[3] I. M. Lifshitz and A. M. Kosevich, J. Exptl. Theoret. Phys. (U.S.S.R.) 29, 730 (1955).

mation on all harmonics. When the approximation $2\pi^2 kT/(e\hbar H/m^*c)\gg 1$ is made and the Dingle[4] factor, x, is included to allow for level broadening due to scattering, then,

$$\chi_\perp = -\frac{4(e\hbar/c)^{\frac{1}{2}}}{(2\pi)^{\frac{3}{2}}\hbar^3}\frac{\partial S_m}{\partial \theta}\left|\frac{\partial^2 S_m}{\partial P_z^2}\right|^{-\frac{1}{2}}\cos\left(\frac{\pi m^*}{m_0}\right)$$

$$\times\frac{kT}{H^{\frac{3}{2}}}\frac{\exp[-2\pi^2 k(T+X)/\beta H]}{1-\exp(-4\pi^2 kT/\beta H)}$$

$$\times\sin\left(\frac{S_m}{e\hbar H/c}\mp\frac{\pi}{4}-2\pi\gamma\right), \quad (2)$$

where β is $e\hbar/m^*c$. The period of this oscillation is then given by

$$P=2\pi e\hbar/cS_m, \quad (S_m \text{ in momentum space})$$

$$=2\pi e/\hbar cS_m = 9.55\times 10^{-9}/S_m(A^{-2}), \quad (S_m \text{ in } k \text{ space}).$$

Although this relation of the periods to the extremal cross section provides a powerful tool for studying the topology of the Fermi surface of metals, a model is required to assign these cross sections to definite locations in the reciprocal lattice and to distinguish between hole and electron cross sections. Very recently Harrison[5] proposed a method for the construction of such models for the Fermi surfaces of polyvalent metals based on the single-orthogonalized-plane-wave (single-OPW) approximation. These models have been extremely successful in predicting the locations and to a somewhat lesser degree the magnitudes of cross-sections of the Fermi surface that will contribute to the DHVA effect in metals like aluminum, lead, magnesium, cadmium, and zinc. For the hexagonal-close-packed metals, however, this construction leads to two possible models, as will be discussed below. The available DHVA effect data on zinc were consistent with the smallest cross sections common to both of these models, but were inadequate to distinguish between the two models. This study was undertaken to complete the low-field DHVA effect measurements in zinc and perhaps determine which one of these models is valid.

[4] R. B. Dingle, Proc. Roy. Soc. (London) A211, 517 (1952).
[5] W. A. Harrison, Phys. Rev. 118, 1190 (1960).

The DHVA effect in zinc was first observed in 1947 by Marcus.[6] At a temperature of 20°K and a magnetic field of 11 kgauss, one damped sinusoid appeared in χ_1. When the experiment was later conducted at liquid-helium temperatures[7-12] and much higher magnetic fields, χ_1 was observed to contain several other periods. The most complete analysis of these periods was done by Verkin and Dmitrenko and later on by Dmitrenko and Lazarev. Their study gave the two sets of long periods as a function of magnetic field orientations with respect to crystalline direction. The other periods, which appear as a complex network of beats, were touched upon but not enough data were reported to give a clear picture of their angular variation.

In the present investigation the torque, C, $(C = \chi_1 H^2)$ exerted by the magnetic field, H, on the specimen is plotted directly versus $1/H$ by an automatic recording circuit. By this method all the fine structures which are essential for accurate analysis of the data can be recorded accurately and efficiently as compared to the point-by-point method by which much of the fine detail of the data can be easily lost.

A total of six sets of periods ranging from 6.3×10^{-5} to 4.8×10^{-8} gauss^{-1} were observed and their angular dependence with respect to crystalline direction determined. They were successfully attributed to portions of the Fermi surface predicted by the single-OPW model. The data, furthermore, indicate what when the field is in the neighborhood of the hexagonal axis, the orbiting electrons do indeed see an energy gap across the hexagonal face of the first Brillouin zone and hence for those field directions, at least, the single-zone scheme must be used. (This will be discussed below in more detail.) Although the angular dependence of these periods agrees well with the model, their magnitudes are in disagreement in some instances by as much as a factor of 10. One then infers that such deviation is caused by distortions of the Fermi surface due to energy gaps, such distortions not being included in the single-OPW approximation.

SINGLE-OPW MODEL FOR THE FERMI SURFACE OF ZINC

The assumptions that the lattice potential is weak and a single-orthogonalized-plane-wave is a fair approximation to the wave function of an electron in the metal give rise to a spherical Fermi surface with connectivity modifications at the Bragg reflection planes. The size

[6] J. Marcus, Phys. Rev. **71**, 559 (1947).
[7] B. I. Verkin and I. M. Dmitrenko, Izvest. Akad. Nauk. S.S.S.R. **19**, 409 (1955) [Columbia Tech. Transl. **19**, 375 (1955)].
[8] I. M. Dmitrenko, B. I. Verkin, and B. G. Lazarev, J. Exptl. Theoret. Phys. (U.S.S.R.) **35**, 328 (1958).
[9] J. S. Dhillon and D. Shoenberg, Phil. Trans. Roy. Soc. (London) **A248**, 1 (1955); L. Mackinnon, Proc. Phys. Soc. (London) **B62**, 170 (1949).
[10] T. G. Berlincourt and M. C. Steel, Phys. Rev. **95**, 1421 (1954).
[11] S. G. Sydoriak and J. E. Robinson, Phys. Rev. **75**, 118 (1949).
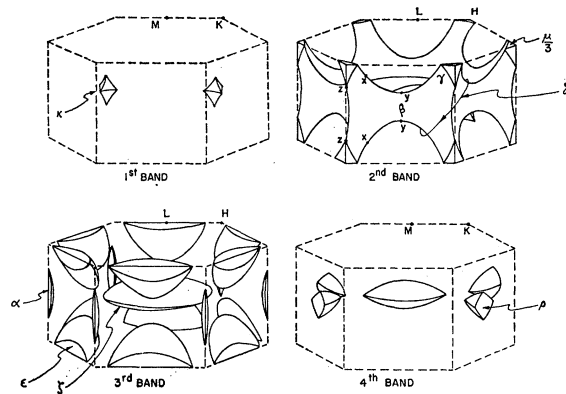[12] T. Fukuroi and Y. Saito, Sci. Repts. Research Inst. Tohoku Univ. **A9**, 273 (1957).

FIG. 1. The nearly free-electron Fermi surface in the reduced single-zone scheme (not to scale). Necessary points of symmetry are shown.

of this surface is determined by the number of free electrons per unit cell. This approximation (see reference 5) proved to be successful in yielding a model for the Fermi surface the properties of which are in fair agreement with the results of the DHVA effect, cylcotron resonance and anomalous skin effect in aluminum,[13] cadmium, zinc,[5] lead,[14] and magnesium.[15]

For the hexagonal-close-packed metals two possible models have been suggested: (1) If no energy gap is assumed to exist across the hexagonal face of the first Brillouin zone, the so-called double-zone[5] scheme is used. (2) When, on the other hand, an energy gap due to spin-orbit splitting[16] is considered to exist between the first and second bands over portions of the hexagonal face, the single-zone scheme (Fig. 1) is used. It may happen, however, that in the presence of a large magnetic field, the electrons are able to penetrate this gap (magnetic breakdown). This penetration becomes important when[17]

$$\hbar\omega_c \gtrsim E_g^2/E_f,$$

where ω_c is the cyclotron frequency, E_g is the energy gap, and E_f is the Fermi energy. For the conditions $\hbar\omega_c \gg E_g^2/E_f$ or $\hbar\omega_c \ll E_g^2/E_f$ either the double- or the single-zone scheme is valid, respectively.

The results of this investigation on zinc favor the single-zone scheme. Therefore this scheme has been used to construct the Fermi surface, Fig. 1, for zinc, a divalent hexagonal-close-packed metal (2 atoms per unit cell).

Some of the various extremal cross-sections that contribute to the DHVA effect are labeled with Greek letters in Fig. 1. In the first band only small hole pockets, κ, exist in the corners of the hexagonal face.

[13] W. A. Harrison, Phys. Rev. **116**, 555 (1959).
[14] A. V. Gold, Phil. Trans. Roy. Soc. (London) **A251**, 85 (1958).
[15] W. L. Gordon, A. S. Joseph, and T. G. Eck, *The Fermi Surface* (John Wiley & Sons, Inc., New York, 1960), p. 84.
[16] M. Cohen and L. Falicov, Phys. Rev. Letters **5**, 544 (1960).
[17] M. Cohen and L. Falicov, Phys. Rev. Letters **7**, 231 (1961); E. I. Blount (to be published).

In the second band, the hole surface contains several sets of extremal cross sections; only those labeled β, γ, δ, and μ have been observed. The extremal cross-sections μ and κ do not appear in the double-zone scheme. The portions of the Fermi surface labeled α, ϵ, and ζ are overlaps in the third band and those labeled ρ are overlaps in the fourth band. Of these, only the portions labeled α are observed in magnetic fields up to 23 kgauss.

EXPERIMENTAL PROCEDURE

The DHVA oscillations in the torque exerted by a magnetic field on the specimen at low temperatures are observed using a null-deflection technique and a torsion apparatus similar to that of Croft, Donahoe, and Love,[18] in conjunction with a metal cryostat of standard design for use in magnetic fields. A 12-in. type 4021-3B Varian magnet, rotatable about a vertical axis, supplied fields up to 23 kgauss where the homogeneity is down by 0.05% over a $\frac{1}{4}$-in. diameter circle.

In order to facilitate the analysis of the data, a recording circuit was installed to plot the torque directly versus the reciprocal of the magnetic field. A block diagram of this arrangement is shown in Fig. 2. The feedback current from the cathode follower of the torque measuring circuit is sampled by a decade resistance box, filtered, and then fed into the X side of a Mosely X-Y recorder. The magnetic field is monitored by a Rawson rotating probe, the output of which is connected to the input of a demodulator where it is amplified, rectified, and then fed into one side of a Wheatstone-type bridge. The step attenuator and 5-kohm helipot in the Y-side of the recorder are electrically disconnected and the signal from the Wheatstone bridge is fed directly to the preamplifier of the Y side which drives the drum. Since the 5-kohm helipot is mechanically driven by the drum, the resistance R_x tapped off the helipot is proportional to the angle of
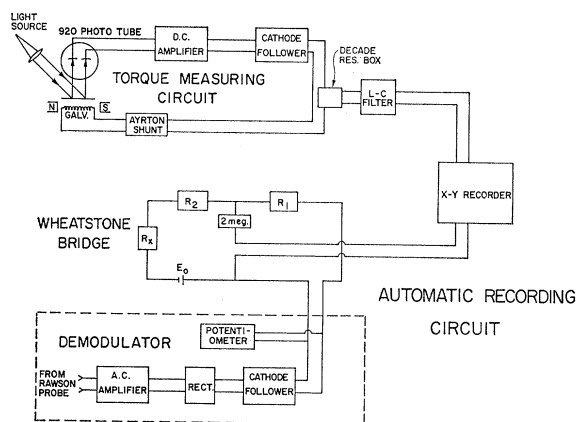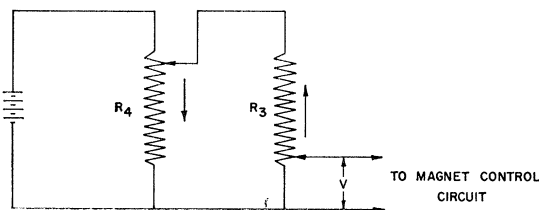

FIG. 3. The magnetic field sweep. R_3 and R_4 are two helipots driven by synchronous motors.

rotation of the drum. With this arrangement the angle of rotation of the drum is inversely proportional to the input voltage from the cathode follower of the demodulator, and hence to H, the constant of proportionality being adjusted to the desired value by the resistances R_1 and R_2.

The field sweep circuit is shown in Fig. 3. R_1 and R_2 are two helipots driven by two synchronous motors in the manner shown. The field is made to vary smoothly and nonlinearly in time by impressing the nonlinearly varying voltage, V, in series with the reference cells in the magnet power supply. Such a nonlinear drive is necessary in order that the rotation of the drum, which varies as $1/H$, be linear in time. The magnetic field is measured to 1% by measuring the voltage from the cathode follower of the demodulator by a potentiometer contained in the demodulator and calibrated against a nuclear magnetic-resonance gauss-meter. In order to avoid gain fluctuation due to temperature variation in the transistorized demodulator, the latter is kept at ice temperature while taking the data and calibrating the field.

SAMPLE PREPARATION

The single crystal boule was grown by the Bridgeman technique from small beads of high purity zinc obtained from the Consolidated Mining and Smelting Company of Canada, Ltd. as 99.998% material; it has a residual resistance ratio of approximately 3000 near the region where the sample was cut. X-ray back-reflection Laue photographs showed no signs of microstructure greater than 0.3°. For a typical run, an approximately 100 mg sample was cut by a string saw etching technique to nearly the desired orientation. The sample was then mounted on a goniometer and oriented exactly by a back-reflection Laue method. It was then lapped gently while still in the goniometer. After etching, the lapped surface was cemented with Duco cement to a Lucite holder. Final deviation from the desired orientation was no more than 0.3°.

EXPERIMENTAL RESULTS AND DISCUSSION

Crystal orientations and other directions are given in reciprocal space to avoid ambiguity in the description of the Fermi surface of this hexagonal close-packed metal. A three vector notation is employed, where the reciprocal vectors $\mathbf{b}_1$ and $\mathbf{b}_2$ lie in the basal plane and

FIG. 2. An automatic recording circuit that plots the torque directly versus the reciprocal of the magnetic field.

[18] G. T. Croft, F. J. Donahoe, and W. F. Love, Rev. Sci. Instr. 26, 360 (1955).
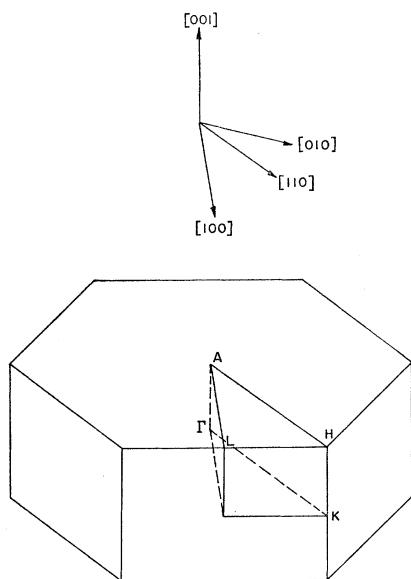
FIG. 4. The first Brillouin zone of hcp structures showing points of symmetry and directions in reciprocal space. The [100] direction coincides with the line ΓM; the [110] direction coincides with the line ΓK.

$60°$ apart while $\mathbf{b}_3$ is normal to this plane. The $\mathbf{b}$ vectors satisfy the relation $\mathbf{a}_i \cdot \mathbf{b}_j = 2\pi\delta_{ij}$ with the primitive translation vectors $\mathbf{a}_i$. Directions in reciprocal space are then stated in terms of the appropriate reciprocal lattice vectors, $\mathbf{K}_m = m_1\mathbf{b}_1 + m_2\mathbf{b}_2 + m_3\mathbf{b}_3$. Using the accepted lattice constants for zinc at room temperature, and the thermal expansion data of Grüneisen and Goens,[19] a c/a ratio of 1.831 was obtained with $a = 2.655$ Å at $4.2°$K. Thus, $|\mathbf{b}_1| = |\mathbf{b}_2| = 2.734$ Å^{-1} and $|\mathbf{b}_3| = 1.293$ Å^{-1} in this work with a free electron sphere radius of 1.586 Å^{-1}.

A total of six sets of periods labeled P_1, P_2, $\cdots$ P_6 in descending order of magnitude were observed in this
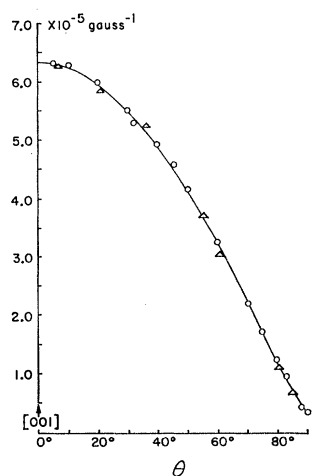
investigation. The measurements were performed for four different specimen orientations with respect to the axis of suspension: (1) the [100], (2) the [110], (3) the [001] directions parallel to the axis of suspension and (4) the [100] direction perpendicular to the axis of suspension, while the [001] direction tilted $28.5°$ away from the horizontal plane. These directions in reciprocal space and their relation to the Brillouin zone are illustrated in Fig. 4.

The longest period was measured in orientations 1 and 2. Both of these orientations yielded the same dependence of P_1 on θ, Fig. 5, where θ is the angle between [001] direction and the magnetic field. At $\theta=0°$, P_1 has a maximum of 6.30×10^{-5} gauss^{-1} and at $\theta=90°$ it has a minimum of 0.378×10^{-5} gauss^{-1}. These values correspond to extremal cross-sections of 0.00015 and 0.0025 Å^{-2}, respectively. Near $\theta=90°$, P_1 was measured at one degree intervals in order to verify the existence of the minimum at $90°$; this is confirmed in Fig. 6.

Harrison attributed this period to the cigar shaped overlaps in the third band labeled α in Fig. 1. According to the model for zinc, these portions of the Fermi surface have a minimum cross section of 0.00030 Å^{-2} and a maximum of 0.0046 Å^{-2}. The agreement of these with the experimental values implies little change in the distance z-z of Fig. 1.

The cyclotron masses for P_1 were calculated to a first approximation from the slope of $\log(C/T)$ versus T plot [see Eq. (2)], and to a second approximation from the plot of $\log(CT^{-1})[1 - \exp(-4\pi^2 kT/\beta H)]$ versus T.
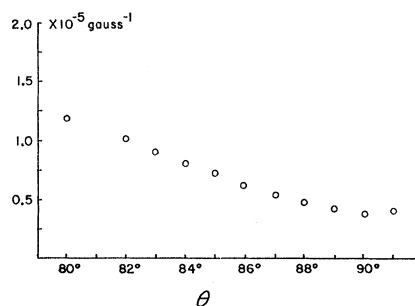

FIG. 5. The angular variation of P_1 with θ, for orientation (1), "O" points, and orientation (2), "$\triangle$" points. P_1 is attributed to those portions labeled α in Fig. 1. The solid curve is the angular dependence of an ellipsoid of revolution with a maximum period of 6.3×10^{-5} gauss^{-1} and a minimum of 0.378×10^{-5} gauss^{-1}.

FIG. 6. Expanded plot of P_1 θ near $\theta=90°$ showing the existence of a minimum at $\theta=90°$.
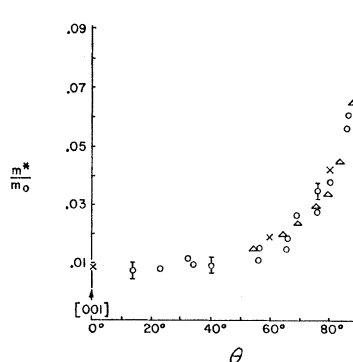

FIG. 7. The cyclotron masses of P_1 versus θ. The theoretical masses, $\times$ points, are compared with the experimental ones, where O points are used for orientation (1) and $\triangle$ points for orientation (2).

[19] E. Grüneisen and E. Goens, Z. Physik 29, 141 (1924).

The results of this calculation are shown in Fig. 7 along with the theoretical effective masses predicted by the single-OPW model (see reference 5 for details). Whenever distortion due to second harmonics occurred in P_1, the calculation of m^* was performed at very low fields where such distortions are negligible.

From the slope of $\log(CH^{-\frac{1}{2}})$ vs H^{-1}, the Dingle scattering factor[4] was calculated for P_1 from $\theta=50°$ to $\theta=89°$; since in this range of θ and for the field values used in this calculation the quantity $\exp(-4\pi^2 kT/\beta H)$ is negligible. When this quantity becomes important for $\theta < 50°$, second harmonics can no longer be neglected and the calculation of x becomes more difficult. Figure 8 shows that near $\theta=90°$ where the extremal cross section of α is maximum, x is large but that it decreases sharply with decreasing cross-section.
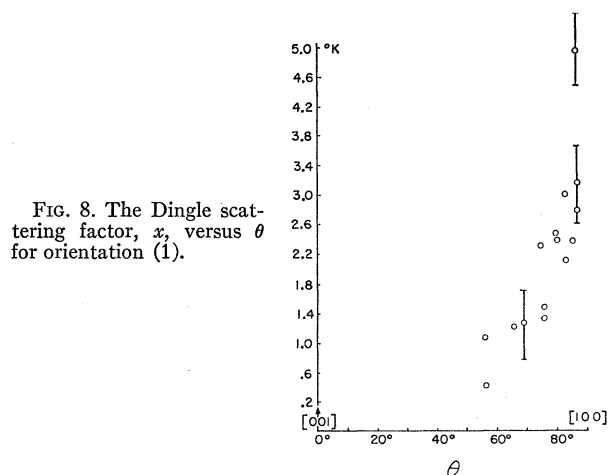

FIG. 8. The Dingle scattering factor, x, versus θ for orientation (1).

A comparison of these values of P_1 to those of other investigators is not presented since it is not relevant to the main point of this paper and would not be meaningful unless accompanied by a more careful study than has yet been undertaken of the factors influencing the size of the α needles. The field dependence of the amplitude of the susceptibility oscillations is qualitatively the same as that reported by other investigators,[7,8,9] dropping below an exponential dependence on a $\log CH^{-\frac{1}{2}}[1-\exp(-4\pi^2 kT/\beta H)]$ versus
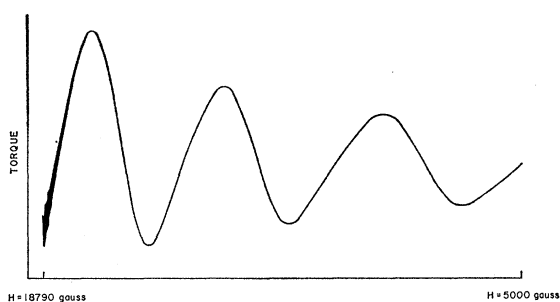

FIG. 9. P_1 at $\theta=45°$ for orientation (1), with P_3 appearing at high H. The field scale is not quite linear in H^{-1}.
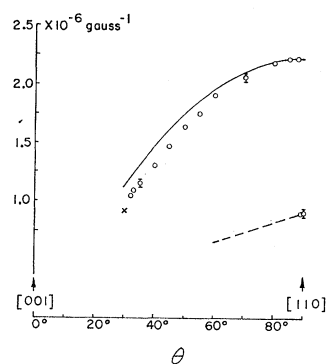

FIG. 10. The angular variation of P_2 with θ, for orientation (1). P_2 is attributed to those portions labeled β in Fig. 1. The solid curve is for an infinite cylindrical segment fitting the maximum of the upper data points. The dashed curve is the expected dependence of P_2 on θ for the β-segment lying 60° from the [110] direction. The point designated by $\times$ is the same as the lower data point at $\theta=90°$ but translated 60° in this figure.

H^{-1} plot with increasing H, as the quantum limit is approached (particularly noticeable for $\theta < 50°$ in the field range studied here). This effect is not well illustrated by Fig. 9 since torque amplitude is plotted just as observed. It is interesting to note that the amplitude of the oscillations in the Ettingshausen-Nernst effect observed by Reynolds, et al.[20,21] do not show this reduction.

The second largest period, P_2, was measured in orientations 1, 2, and 3. The results for each orientation are shown in Figs. 10, 11, and 12, respectively. In Fig. 12, ϕ is the angle in the basal plane between the [$\bar{1}00$] direction and the magnetic field. The angular dependence of P_2 in cases 1 and 3 is seen to be almost identical. The maximum period observed in these cases is 2.24×10^{-6} gauss^{-1}, corresponding to a minimum cross section of 0.0043 Å^{-2}.
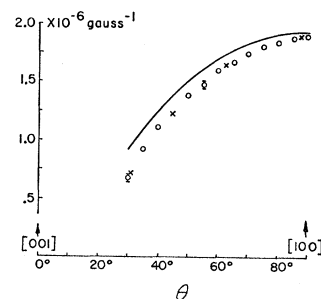

FIG. 11. P_2 versus θ for orientation (2). For several field settings the angle between the [110] direction and the magnetic field is calculated and the period corresponding to this angle is obtained from the upper data points of Fig. 10 and designated by $\times$ in this figure. The solid curve is for an infinite cylinder whose axis is in the [110] direction with a maximum period of 2.24×10^{-6} gauss^{-1}.

[20] K. S. Balain, C. G. Grenier, and J. M. Reynolds, Phys. Rev. 119, 935 (1960).

[21] C. J. Bergeron, C. G. Grenier, and J. M. Reynolds, Phys. Rev. 119, 925 (1960).

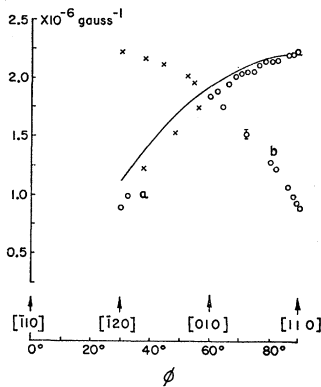FIG. 12. P_2 versus ϕ for orientation (3), where ϕ is the angle between the [$\bar{1}10$] direction and H. The points labeled $\times$ are the reflection of the data points about $\phi=60°$. The solid curve is for an infinite cylinder fitting the maximum of P_2.

FIG. 14. The cross section of the Fermi surface in the (001) plane. At $\phi=26°$ planes perpendicular to H cut large extremal areas through β. Such large cross sections were not observed.

Harrison attributed this period to the hole portions of the Fermi surface in the second band labeled β in Fig. 1, which have a minimum cross-sectional area of 0.045 Å^{-2} in the [110] direction. Six of these segments lie in a plane parallel to the hexagonal face of the Brillouin zone so that when the specimen is suspended as in case 3, the angular dependence of the resulting periods is as shown in Fig. 12. The large deviation of the single-OPW value of the β cross-section from the experimental value implies the existence of large energy gaps in this region. The solid curves in Figs. 10–12 show the angular dependence of a period for an infinite cylinder of a minimum cross section given by the maximum value of P_2. The fact that the experimental points fall below the solid curves indicates that the surface varies hyperbolically as the angle between the magnetic field and the [110] direction is increased; this is consistent with the model. In the neighborhood of $\theta=90°$ in case 1 a smaller period is observed (lower curve in Fig. 10) and attributed to the β in the basal plane 60° from the [110] direction. This smaller period agrees, as it should with the upper curve in Fig. 10 for θ near 30°. For $\theta\leqslant45°$ and $\phi\leqslant26°$ in cases 1 and 3 the cross sections of β by planes perpendicular to the magnetic field should, according to the model, suddenly become large (see Fig. 14 which illustrates this situation for orientation 3). This would result in discontinuities in curves "a" in Figs. 10 and 12. In case 3, P_2 is not observed below 30°. In case 1, however, no discontinuity
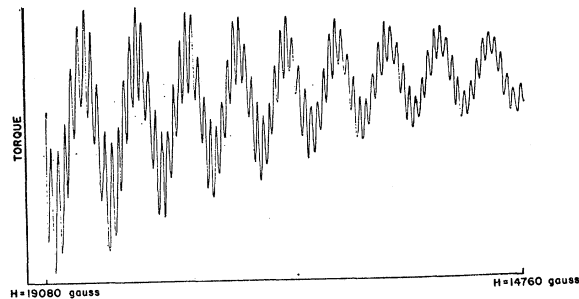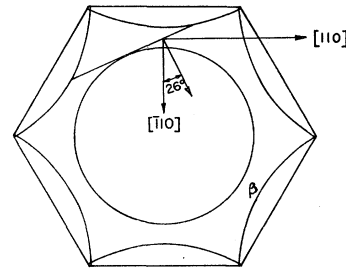
is observed even at $\theta=30°$, which implies that the distance x-x is considerably smaller than that expected from the model. The disappearance of P_2 below $\theta=30°$ could be attributed either to its vanishing amplitude or to the inability at these fields to observe the large cross sections responsible for the expected discontinuity in P_2.

Cyclotron masses as calculated from the data are compared in Fig. 15 with those predicted by the model. This agreement between theoretical and experimental effective masses is surprising in view of the factor-of-10 discrepancy between the experimental and theoretical cross section of β.

The third period is reliably analyzed in the ranges $0°\leqslant\theta\leqslant7°$ and $28°\lesssim\theta\leqslant90°$, for in these regions P_3 is either pure or contains well-defined beats. In the region $7°\lesssim\theta\lesssim28°$, P_3 contains as many as four types of beats which in some cases become extremely difficult to analyze. (The occurrence of such beats is responsible for the relatively large uncertainties assigned to P_3 in this region.) Thorough data were taken in this complex region: some at low fields and a temperature of 4.2°K where the longer periods are usually dominant, and then at high fields and low temperatures where the shorter periods become countable. Once one or two periods are determined, the others are obtained by matching certain parts of a data graph on an analog computer. Thus P_3 is found for the values of θ in orientations 1 and 2, Figs. 16 and 17. A maximum period of 2.25×10^{-7} gauss^{-1} corresponding to a minimum area of 0.0426 Å^{-2} is observed for P_3 in case 1 at $\theta\approx28°$.

P_3 is attributed to those portions of the Fermi surface labeled γ in Fig. 1 and referred to as the arms. These,

FIG. 13. P_2 (larger period) and P_3 in orientation (4) at $\psi=45°$, where ψ is the angle between the [100] direction and the magnetic field. The torque is plotted approximately versus $1/H$.
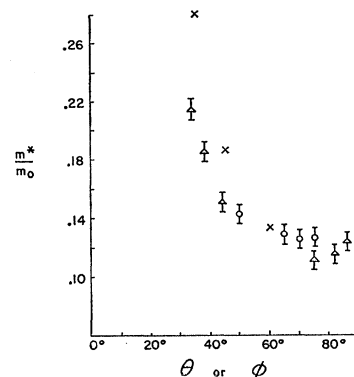

FIG. 15. The theoretical cyclotron masses of P_2 calculated for orientation (3), $\times$ points, are compared with the experimental masses for orientation (1), $\circ$ points, and orientation (3), $\triangle$ points.

according to the model for a c/a ratio of 1.831, have a minimum cross section of 0.06 Å^{-2} at an angle of 28.5° from the hexagonal axis in the [110] direction. If then, the crystal is suspended as in case 1, two arms will lie in a horizontal plane containing the [001] direction, each making an angle of 28.5° with this direction. This pair of arms will contribute curves "a" and "d" of Fig. 16. Curves "b" and "c" are due to the other two pairs of arms. When the specimen is suspended as in case 2, the magnetic field never lies along the normal to the minimum γ cross sections and hence the maximum period of Fig. 17 curve "e" is smaller than that of curve "a" Fig. 16. Curves "e," "f," and "g" of Fig. 17 are due to the three pairs of arms lying symmetrically about the horizontal plane. The solid curves are the angular dependence of a cylindrical surface with a minimum cross section of 0.0426 Å^{-2}. P_3 cannot be attributed to shrunken versions of the ϵ segments of
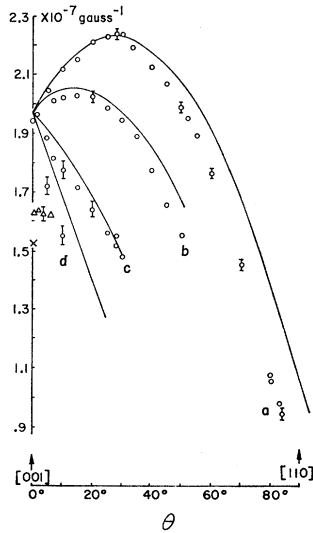

FIG. 17. P_3, O points, versus θ in orientation (2). The $\triangle$ and $\times$ points are for P_4 and P_5 respectively. The solid curves are for an infinite cylinder representation of the arms as viewed in orientation (2).

FIG. 16. The angular variation of P_3, O points, with θ for orientation (1). The $\triangle$ and $\times$ points are for P_4 P_5, respectively. P_3, P_4, and P_5 are attributed respectively to those portions labeled γ, κ, and μ in Fig. 1. The solid curves are for infinite cylinders fitting the maximum of P_3 and oriented in the same direction as the various arms.

Fig. 1 even if these are distorted to give a minimum extremal cross section near $\theta = 28°$ because such a minimum would be observed when the crystal is suspended as in orientation (2).

As can be seen from curve "a" of Fig. 16, P_3 is not symmetrical about $\theta = 28.5°$. Such asymmetry is also apparent from the manner in which each data curve deviates from the corresponding solid curve. Any decrease of the angle between the [001] and the cylinder axes to improve the fit to curve "a", pulls the other solid curves farther from the data of Fig. 17. However, greater asymmetry is expected from the model, for in the vicinity of the hexagonal axis the model predicts that planes normal to the magnetic field will cut a large area including more than one arm via the bridge between the arms. Consequently curve "a" of Fig. 16, for example, should, according to the model, cut off at $\theta \leqslant 7°$ and most of curve "b" and all of "c" and "d"
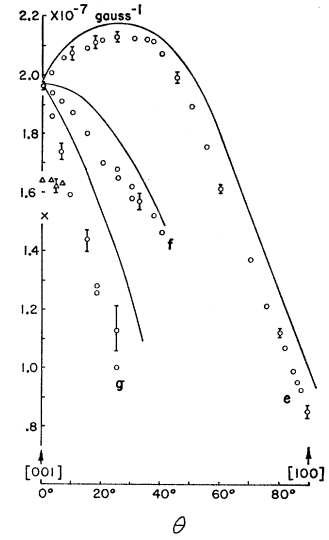
should disappear completely. However, as confirmed by the results of P_2, the distances x-x and y-y are smaller then those expected from the model. Therefore, planes perpendicular to the magnetic field will no longer intercept large areas via the bridge even if, as implied by the results of P_1, the distance z-z is nearly that of the model. In this way, the existence of P_3 at small θ, Figs. 16 and 17, can be explained.

The experimental cyclotron masses are calculated for only two values of θ because the oscillations without beats and with accurately measurable amplitude appear over a small region as illustrated in curve "a" of Fig. 16 and curve "e" of Fig. 17.

	Exp.	Theor.
$\theta = 63°$	$m^*/m = 0.154$	0.172
$\theta = 78°$	$m^*/m = 0.22$	0.33

The shortest period observed, P_6, is shown in Figs. 18 and 19. When the [110] direction is parallel to the axis of suspension, P_6 has a maximum of 4.8×10^{-8} gauss^{-1} at $\theta = 40°$ which corresponds to a minimum area of 0.2 Å^{-2}. Because the amplitude of P_6 is small, it is masked in all directions by P_3. By tilting the sample so that the [001] direction is about 2° off the horizontal
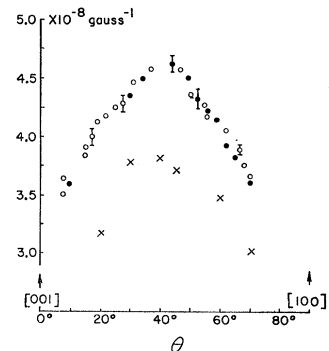

FIG. 18. The angular varition of P_6 with θ for orientation (2). Data for two separate runs are shown by the filled and open circles. The assignment of error bars is based on the uncertainty in counting periods. The $\times$ points are the periods predicted for the δ segments of Fig. 1.
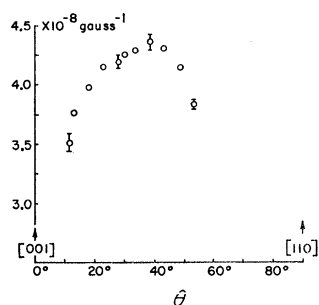
FIG. 19. P_6 versus θ for orientation (1).

plane, long-waisted beats in P_3 occur, thereby facilitating the study of P_6 in these waists. A sample of such results is shown in Fig. 20

The only portion of the model found to minimize near $\theta \approx 40°$ is that labeled δ in Fig. 1. The theoretical angular dependence of the period predicted for this cross section as shown in Fig. 18 by the "x" points is in good agreement with the experimental results. Therefore P_6 is attributed to the δ segments.

The last two periods P_4 and P_5, designated by $\triangle$'s and $\times$'s in Figs. 16 and 17 are observed in the vicinity of the [001] direction at which they have the values 1.64×10^{-7} gauss^{-1} and 1.52×10^{-7} gauss^{-1} corresponding to extremal areas of 0.058 Å^{-2} and 0.063 Å^{-2}. P_4 is determined up to $\theta \approx 7°$ whereas P_5 is observed only in the immediate vicinity of the [001] direction and occurs as a modulation of the amplitude of P_3. This type of modulation may be caused either by a period of 2.46×10^{-7} gauss^{-1} or by one of 1.52×10^{-7} gauss^{-1} when superimposed on P_3. The latter value is chosen for the reasons discussed in reference 22. Beyond $\theta = 7°$, P_4 is not distinguishable from P_3, but careful study of the data shows that it is not present at $\theta \geqslant 15°$. The presence of P_4 is illustrated in Fig. 21.

All the periods, other than P_4 and P_5, so far discussed, have been attributed to portions of the Fermi surface which are common to the single and double zone scheme
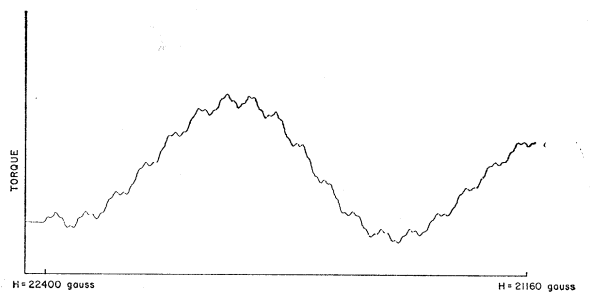

FIG. 20. P_6 (shortest period), P_3, and P_2 at $\theta = 68°$ in orientation (1). At this value of θ, P_6 can be counted more accurately than at most other field orientations, as illustrated by error bars in Figs. 18 and 19.

[22] A. S. Joseph, W. L. Gordon, J. R. Reitz, and T. G. Eck, Phys. Rev. Letters 7, 334 (1961).

models. P_4 and P_5, however, cannot be attributed to any obvious cross sections in the double-zone model, but do fit naturally with the cross sections in the single-zone scheme labeled κ and μ in Fig. 1. Further confirmation of this assignment is given by a recent band structure calculation by Harrison,[23] which fits other cross sections observed in zinc. He obtains a value of 0.058 Å^{-2} for the average cross section of μ and κ in the [001] direction as compared with the experimental value of 0.061 Å^{-2}.

The observation of P_4 and P_5 is convincing evidence of a spin-orbit energy gap over portions of the hexagonal face of the first Brillouin zone. The fact that they occur in the region near the [001] direction, does not necessarily imply the validity of the single zone scheme in all directions. It is quite conceivable that beyond $\theta = 10°$ the angle between the electron orbit and the hexagonal face of the Brillouin zone is sufficient at these fields to
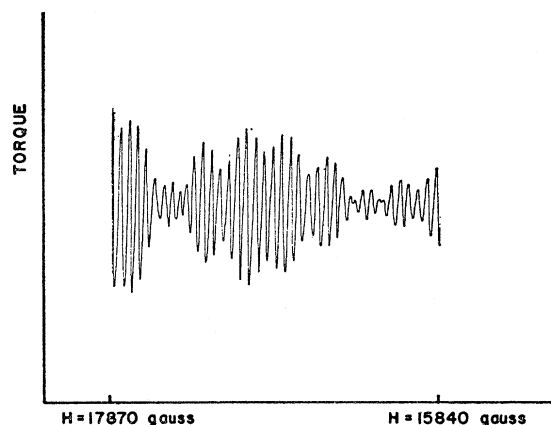

FIG. 21. P_4 at $\theta = 3°$ in orientation (2). The long beat is due to the arms periods, P_3. The shorter beats are due to the presence of P_4 together with the components of P_3.

allow magnetic breakdown[16,17] to occur in which case the double-zone scheme becomes valid.

The specimen was also suspended as in orientation 4 to investigate the possible existence of any new sets of periods. No such new periods were observed.

CONCLUSION

The model of the Fermi surface of zinc as obtained from a single-OPW approximation is in excellent qualitative agreement with the measurements of this investigation. The observation of holes in the first band, κ, and the arms junctions, μ, in the second band support the validity of the single-zone scheme, at least for field settings of $\theta = 0°$ to $\theta \approx 10°$. Beyond $\theta \approx 10°$ magnetic breakdown may occur in which case the double-zone scheme is appropriate.

The cross sections predicted by the model, that have

[23] W. A. Harrison, following paper [Phys. Rev. 126, 497 (1962)].

not been observed, are ϵ and ζ in the third band and ρ in the fourth. The periods expected from these cross sections are of the order of magnitude of P_6, the δ cross section. A weak beating in P_6 has been observed and therefore may have been indicative of the presence of such periods. However, positive identification could not be made because of the distortion caused by P_3, which occurs with an amplitude much larger than that of P_6. With higher fields and higher specimen purity these cross sections should be determinable.

Band Structure and Fermi Surface of Zinc

WALTER A. HARRISON
General Electric Research Laboratory, Schenectady, New York
(Received November 27, 1961)

The band structure of zinc is calculated using a modified orthogonalized-plane-wave method and the Hartree-Fock calculations of neutral zinc by Piper. The band structure is obtained in a form which allows it to be extended readily to slight distortions of the lattice. The calculated structure is compared to an experimental band structure obtained by adjusting the matrix elements to fit de Haas-van Alphen observations of the zinc Fermi surface. The band energies do not differ by more than 0.04 ry for the two treatments. The Fermi surface from the experimental band structure is drawn in some detail. One matrix element is found to be only 0.004 ry, requiring an analysis of magnetic breakdown in the interpretation of experiments. The probability of band-to-band transitions, calculated explicitly in the high-field limit, is continued into the low-field range with a result equivalent to Blount's low-field result. The formulas for the intermediate range are applied to zinc.

I. INTRODUCTION

THE motivation for undertaking a detailed band-structure determination is based on several major changes in the nature of our understanding of the electronic structure of metals:

(a) Extensive experimental work[1] has established in some detail and with some precision the size and shape of the Fermi surfaces in several metals.

(b) Band-structure calculations[2-6] have in several cases given a very good account of the Fermi surfaces determined experimentally.

(c) New techniques[3,7,8] make it possible to obtain the essentials of the band structure without recourse to the large amounts of effort and expense previously necessary.

(d) The discovery[1] that many of the polyvalent metals have band structures which do not deviate greatly from a free-electron or one-OPW (orthogonalized-plane-wave) approximation gives hope that simplified approaches may allow one to treat the modifications in band structure which occur due to lattice distortions and alloying.

In this framework, it appeared appropriate to explore the influence of the band structure on various metallic properties. It was first desirable to establish with some certainty the band structure of an individual polyvalent metal; both from a full band calculation and from experimental studies of the Fermi surface. If reasonable agreement between the two were obtained, one might have some confidence in the structure, and proceed to study the influence of this structure on various properties of the metal.

In selecting a metal, it was decided that the extra richness in properties for a hexagonal metal favored it over a cubic metal. Of the hexagonal metals, zinc has been most thoroughly studied experimentally and its c/a ratio deviates appreciably from that for close packing, a fact which would be interesting to explore. Furthermore, it was necessary to start from scratch in order to obtain the flexibility which would make it possible to examine changes in band structure under modifications of the lattice. Since a band structure calculation has

[1] *The Fermi Surface*, edited by W. A. Harrison and M. B. Webb (John Wiley & Sons, Inc., New York, 1960).

[2] V. Heine, Proc. Roy. Soc. (London) A240, 340, 361 (1957), aluminum.

[3] W. A. Harrison, Phys. Rev. 118, 1182 (1960), aluminum.

[4] B. Segall, Phys. Rev. Letters 7, 154 (1961), copper; Phys. Rev. 125, 1797 (1961), aluminum; (to be published), silver and gold.

[5] G. A. Burdick, Phys. Rev. Letters 7, 156 (1961), copper.

[6] L. Falicov (to be published), magnesium.

[7] J. C. Phillips and L. Kleinman, Phys. Rev. 116, 287, 880 (1959).

[8] M. H. Cohen and V. Heine, Phys. Rev. 122, 1821 (1961).